Accepted Manuscript

Pyridostatins Selectively Recognize Two Different Forms of the Human Telomeric G-Quadruplex Structures and Their Anti-tumor Activities in Vitro

Li-Xia Wang, Qian Shang, Qian Li, Jun-Feng Xiang, Yan Liu, Ai-Jiao Guan, Hong-Xia Sun, Li-Jia Yu, Ya-Lin Tang

PII: S0040-4020(15)00788-7

DOI: 10.1016/j.tet.2015.05.081

Reference: TET 26799

To appear in: *Tetrahedron*

Received Date: 23 March 2015

Revised Date: 19 May 2015

Accepted Date: 22 May 2015

Please cite this article as: Wang L-X, Shang Q, Li Q, Xiang J-F, Liu Y, Guan A-J, Sun H-X, Yu L-J, Tang Y-L, Pyridostatins Selectively Recognize Two Different Forms of the Human Telomeric G-Quadruplex Structures and Their Anti-tumor Activities in Vitro, *Tetrahedron* (2015), doi: 10.1016/j.tet.2015.05.081.

Graphical Abstract

To create your abstract, type over the instructions in the template box below.
Fonts or abstract dimensions should not be changed or altered.

Pyridostatins Selectively Recognize Two Different Forms of the Human Telomeric G-Quadruplex Structures and Their Anti-tumor Activities in Vitro

Leave this area blank for abstract info.

Li-Xia Wang, Qian Shang, Qian Li, Jun-Feng Xiang, Yan Liu, Ai-Jiao Guan, Hong-Xia Sun, Li-Jia Yu, Ya-Lin Tang*

State Key laboratory for Structural Chemistry of Unstable and Stable Species, Institute of Chemistry, Chinese Academy of Sciences (ICCAS), Beijing 100190, China.

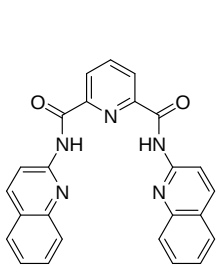

Pyridostatin I

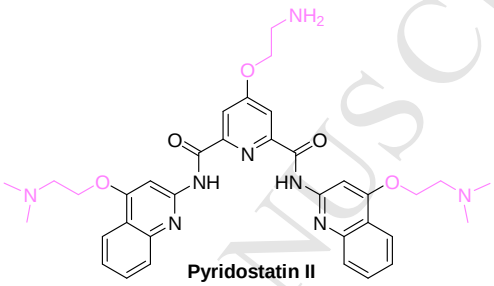

Pyridostatin II

Tetrahedron
journal homepage: www.elsevier.com

Pyridostatins Selectively Recognize Two Different Forms of the Human Telomeric G-Quadruplex Structures and Their Anti-tumor Activities in Vitro

Li-Xia Wang [a], Qian Shang [a], Qian Li [a], Jun-Feng Xiang [a], Yan Liu [a], Ai-Jiao Guan [a], Hong-Xia Sun [a], Li-Jia Yu [a], Ya-Lin Tang [a,*]

[a] *Beijing National Laboratory for Molecular Sciences (BNLMS), Center for Molecular Sciences, State Key Laboratory for Structural Chemistry of Unstable and Stable Species, Institute of Chemistry Chinese Academy of Sciences, Beijing 100190, P.R. China. E-mail: tangyl@iccas.ac.cn; Fax: 86-10-6252-2090; Tel: 86-10-6252-2090.*

ARTICLE INFO

Article history:
Received
Received in revised form
Accepted
Available online

Keywords:
G-quadruplex
recognition
stabilization
pyridostatin derivatives
anti-cancer drug

ABSTRACT

G-quadruplex as a therapeutic target to develop novel anti-cancer agents has attracted a growing interest. Among all the ligands of G-quadruplexes, pyridostatin derivatives play a very important role. Here, we first reported the recognition of the fundamental skeleton pyridostatin **I**, which was simply synthesized. Compared to pyridostatin **II** comprising terminal amino groups, pyridostatin **I** selectively stabilized intramolecular anti-parallel telomeric G-quadruplex by raising the melting temperature about 20 °C at 295 nm of H22, while pyridostatin **II** preferred to stabilize intermolecular parallel telomeric G-quadruplex by raising the melting temperature about 25 °C at 265 nm of H7, maybe due to the suited size measurements between G-quadruplex hosts and pyridostatin guests. MTT assays indicated that pyridostatin **II** had better cytotoxic effects against HCT-8 and A549 cell lines obviously, indicating positively charged side chains may be required for improving the water solubility and cellular uptake of the apolar central skeleton.

1. Introduction

Telomeres are essential chromosomal components to protect the end of eukaryotic chromosomes and maintain proper replication.[1] The G-quadruplex structure formed by human telomeric DNA repeats has been witnessed to inhibit telomerase activity in vitro.[2-4] G-tetrad of G-quadruplex is a square planar alignment of four guanines connected by cyclic Hoogsteen hydrogen bonding of guanine bases and plays a very important role in recognizing planar aromatic ligands through π-π stacking mainly, that brings the ligands into, or very close to, the G-quadruplex host.[5-9] Molecules that induce and stabilize G-quadruplex structures have the potential to interfere with telomere replication and serve as anti-cancer agents.[10-15] Therefore, there are growing interests on G-quadruplex as a therapeutic target to develop novel anti-cancer agents.

Unlike dsDNA, G-quadruplex exhibits structural polymorphism depending on the number of strands involved in the structure, strand orientation and variations in loop size and sequence.[16] G-quadruplex structures could be summarized by three conformation: anti-parallel, parallel, and hybrid-type with both parallel and anti-parallel features. Human telomeric nucleotide sequence can provide all the three different conformations. For example, four T7 d(TTGGGTT) stands could bind together to form an intermolecular parallel G-quadruplex structure.[17] A single DNA H24 d(TTAGGG)$_4$ give intramolecular G-quadruplexes: an anti-parallel conformation in the presence of Na^+, a parallel conformation in the presence of PEG200, and a hybrid-type conformation in the presence of K^+.[18-21] The conformer of G-quadruplex plays an important role in providing special sites for recognition of small-molecule ligands, to be applied in assisting the catalytic transformation[22]

* Corresponding author. Tel.: +010-62622090; fax: +010-82617304; e-mail: tangyl@iccas.ac.cn.

and designing new anti-cancer agents.[10-15] Pyridostatin derivatives comprising terminal amino groups have been designed to promote the folding of telomeric G-quadruplexes.[23-24] So far as we know, what role does the fundamental skeleton pyridostatin **I** (Scheme 1) play in recognizing G-quadruplex has never been described. For comparison, we also successfully prepared another new molecule pyridostatin **II**, which contained a (2-dimethylamino)ethoxy group linked to each quinoline fragment without no need of amino-protection, but the structure was similar to the reported probe by Balasubramanian et. al.[23-24] In our research, we found that pyridostain **I** selectively stabilized intramolecular anti-parallel telomeric G-quadruplex, whereas pyridostatin **II** with terminal amino groups stabilized intermolecular parallel telomeric G-quadruplex.

2. Results and Discussion

Telomeric sequences d[TTAGGGT] (H7) and d[AGGG(TTAGGG)$_3$] (H22) have been chosen to prepare the various conformations of telomeric G-quadruplexes. CD spectra has been first used to confirm the effect of pyridostatin derivatives on the conformational transition of telomeric G-quadruplexes. The CD spectra of parallel G-quadruplexes showed a negative band at 240 nm and a positive band at 265 nm; anti-parallel G-quadruplexes showed a negative band at 260 nm and a positive band at 295 nm; and hybrid-type G-quadruplexes showed a negative band at 240 nm and two positive bands at 265 and 290 nm. The addition of pyridostatin **I-II** did not cause a transition of the CD spectra of all the telomeric G-quadruplexes investigated, indicating that pyridostatin **I-II** did not alter the conformations, which facilitates the study on telomeric G-quadruplexes recognition of pyridostatin **I-II**. The synthetic pathways for new pyridostatin **I-II** are shown in Experimental Section, and some key intermediates of pyridostatin **II** are shown in Supporting Information.

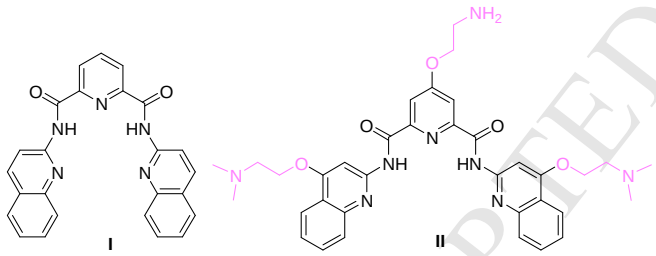

Scheme 1. Structures of pyridostatin **I** and **II**.

Selectively Recognition for Different Telomeric G-Quadruplexes of Pyridostatin I and II.

Circular Dichroism Spectroscopy

Pyridostatin **I** as a neutral molecule was prepared from one-step reaction between 2,6-pyridinedicarbonyl dichloride and 2-aminoquinoline. To evaluate the effect of pyridostatin **I** on the telomeric G-quadruplexes, we applied circular dichroism to monitor the melting temperature (T_m) of Hum G-quadruplexes. The change of T_m in the folded and unfolded quadruplex structure upon interacting with ligand provides evidence of thermal stabilization of DNA structure. Telomeric G-quadruplex was incubated with pyridostatin **I** at 2 equal molar ratio for more than 12 h, the T_m values for varied G-quadruplexes were calculated as shown in Fig.1a. The pyridostatin **I** shows the preference for the intramolecular anti-parallel G-quadruplex, and selectively stabilizes G-quadruplex H22, raising the melting temperature about 20 °C monitored at 295 nm. Whereas, pyridostatin **I** shows weak ability to stabilize parallel intramolecular G-quadruplex H7 by raising the melting temperature about 5 °C. In the contrast, pyridostatin **II** shows a strong ability to stabilize G-quadruplex H7 by raising the melting temperature about 25 °C, but a weak ability to stabilize G-quadruplex H22.

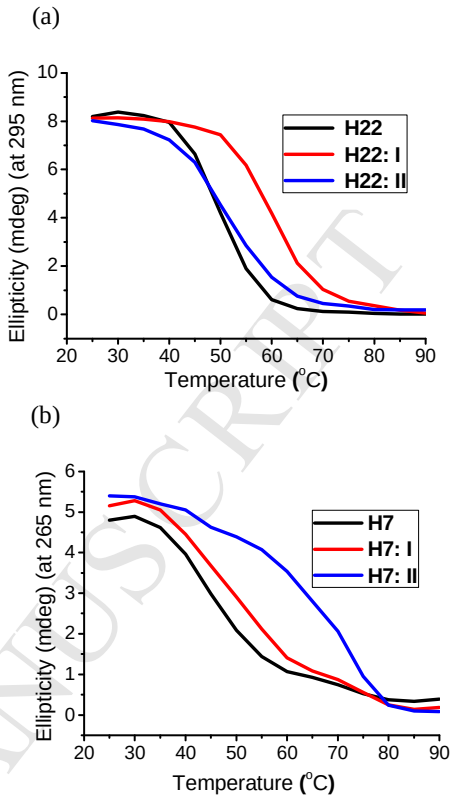

Fig. 1. CD melting profiles of: (a) G-quadruplex of H22 (5 μM) with pyridostatin **I** or **II**; (b) G-quadruplex of H7 (5 μM) with pyridostatin **I** and **II** in Tris-HCl buffer (20 mM, pH 7.4, 100 mM NaCl).

Fluorescence Spectroscopy

The fluorescence spectra of pyridostatin **I** and **II** binding with intramolecular and intermolecular telomeric G-quadruplexes are respectively given in Fig. 2. The interaction of pyridostatin **I-II** with these G-quadruplexes resulted in concomitant discrepancy on their spectra. The increasing amout of DNA led to the gradual quenching of fluorescence emissions in Tris-HCl buffer. For intermolecular parallel G-quadruplex H7, the presence of which with more than 4 equiv. relative to pyridostatin **I** led to the obivious discrepancy. While, intramolecular anti-parallel G-quadruplex H22 with the ratio of 1:1 gave nearly no peak at λ_{em} = 444 nm of pyridostatin **I**. For pyridostatin **II**, both of the chosen telomeric G-quadruplexes H7 and H22 led to its decrease of the fluorescence intensity at 361 nm, but the H7 was the better one. These results clewed that pyridostatin **I** selectively recognized intramolecular anti-parallel G-quadruplex over intermolecular parallel G-quadruplex, while pyridostatin **II** prefered to recognize intermolecular parallel G-quadruplex.

(a)

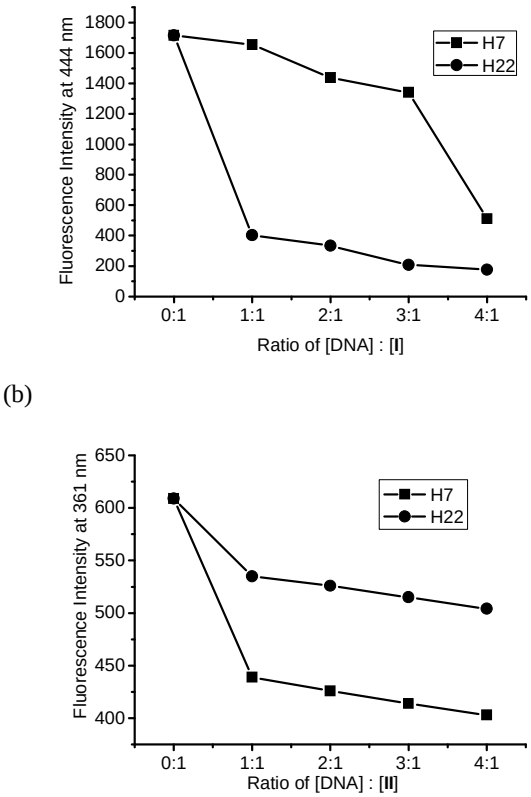

Fig. 2. The fluorescence emission spectra of pyridostatin **I** (3 μM) and its complexes with (a) intermolecular parallel G-quadruplex H7 and (b) intermolecular anti-parallel G-quadruplex H22 in Tris-HCl buffer (20 mM, pH 7.4, 100 mM NaCl).

Binding modes of pyridostatin derivatives targeting to telomeric G-quadruplexes.

Pyridostatin**s** showing different preference for human telomeric G-quadruplex structures, prompted us to investigate the binding modes between pyridostatins and G-quadruplex structures. To investigate the binding modes between pyridostatin **I-II** and intermolecular or intramolecular G-quadruplex structure, qualitative molecular modeling using molecular mechanics energy minimizations was studied.

Optimized models of the complexes between pyridostatin **I-II** and G-quadruplexes H22 or H7 were illustrated in Fig. 3. Molecular modeling in the ratio of 1:1 shows that the end-stacking mode is favored for pyridostatin **I** binding to the intramolecular G-quadruplex H22 while the groove binding mode is favored for pyridostatin **II** binding to the intermolecular G-quadruplex H7, the binding energy was -59.93 kcal/mol and -66.62 kcal/mol, respectively. In comparision, the binding energy for pyridostatin **I** binding to the G-quadruplex H7 was -45.32 kcal/mol (Fig. S1a); while the binding energy for pyridostatin **II** binding to the G-quadruplex H22 was -56.27 kcal/mol (Fig. S1b). Although the pyridostatin **I** and **II** showed similar interaction mode and non-bonded interaction energy, the torsional energy of the pyridostatin **II** was much higher than pyridostatin **I**. The relatively high torsional energy made the pyridostatin **II** unstable when binding to the intramolecular G-quadruplex H22. Therefore, the pyridostatin **I** was more favored binding to intramolecular G-quadruplex H22 than the pyridostatin **II**. Whereas, the pyridostatin **II** had a preference for intermolecular G-quadruplex H7, the multi-amino-appendages of which endowed with positive charges made good matches with the shape and volume of the G-quadruplex H7 active sites.

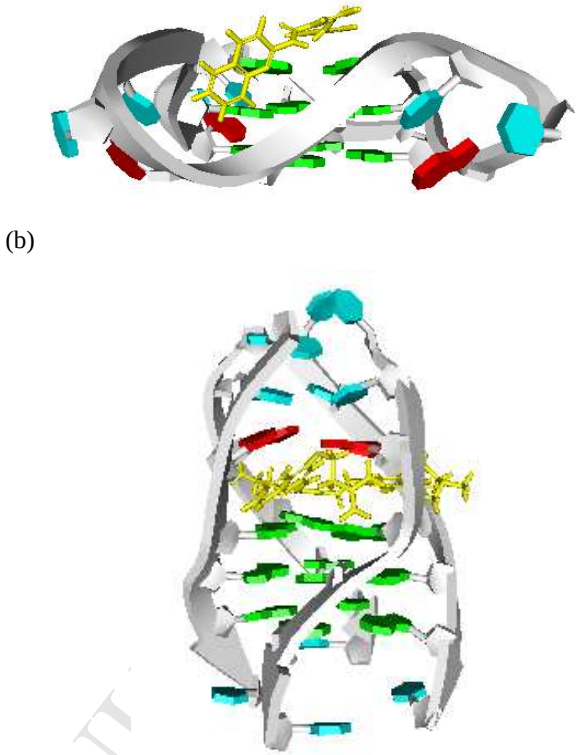

Fig. 3. Optimized models of: (a) complex between pyridostatin **I** and H22 anti-parallel G-quadruplex; (b) complex between pyridostatin **II** and H7 parallel G-quadruplex. The G is colored in green, the T is colored in light blue, the A is colored in red, and the ligands are colored in yellow.

The anti-tumor activities of pyridostatin I-II.

Considerable circumstantial evidence suggests that these structures can exist *in vivo* in specific regions of the genome including the telomeric ends of chromosomes and oncogene regulatory regions. Recent studies have demonstrated that small molecules can facilitate the formation of, and stabilize, G-quadruplexes. In our research, pyridostatin **I** and **II** showed the discrepant recognition of telomeric G-quadruplex, thus possibly led to the different inhibition of anticancer cells. IC_{50} values i.e., the effective concentration at which 50% growth of the cancer cells was inhibited, were calculated to evaluate the anticancer activities. Human colonic carcinoma cell line (HCT-8), human non-small cell lung cancer cell line (A549), and human hepatocellular carcinoma cell line (BEL-7402) were used in the cytotoxicity test. All the experiments were carried out in triplicates, and the results were shown in Table 1.

Table 1. IC_{50} values of pyridostatin **I** and **II** on human cancer cell lines.[a]

Compound	IC_{50} values in μM		
	HCT-8	BEL-7402	A549
I	> 100	> 100	> 100
II	9.19 ± 0.18	> 100	4.66 ± 0.64
5-Fu	87.33 ± 0.93	53.97 ± 0.30	69.96 ± 1.87

a IC_{50} is the drug concentration effective in inhibiting 50% of the cell growth measured by the MTT assay after 72 h drug exposure.

As shown in Table 1, pyridostatin **II** shows significant cytotoxic activities on HCT-8 and A549 cell lines, better than **I** and 5-Fu (positive control), but little effect on BEL-7402, maybe related to the content and the types of telomeric G-quadruplexes

in the chosen samples.[29] Pyridostatin **I** doesn't give good results as a cancer inhibitor, maybe due to the limited solubility in water leading to the very high IC_{50} values, and meanwhile indicates that multi-amino appendages on pyridostatin **II** providing positively charged side chains may be required for improving the water solubility and cellular uptake of the apolar central skeleton.

3. Conclusion

In summary we have identified two new pyridostatin compounds **I** and **II** as potent G-quadruplex stabilizing small molecules. Pyridostain **I** selectively stabilized intramolecular anti-parallel G-quadruplex H22, whereas pyridostatin **II** with terminal amino groups stabilized intermolecular parallel G-quadruplex H7, maybe due to the suited size measurements between G-quadruplex hosts and pyridostatin guests. MTT assays indicated that pyridostatin **II** had good cytotoxic effects against HCT-8 and A549 cell lines, and had a potential application in the exploration of anticancer drugs.

4. Experimental Section

4.1. Compounds and Materials

Preparation of pyridostatin **I**.

Pyridostatin **I** was prepared from the reaction between 2-aminoquinoline (1.40 g, 9.50 mmol) and 2,6-pyridine dicarbonyl dichloride (1.00 g, 4.75 mmol) in 40 mL of dry toluene under reflux for 4 hours (Scheme 2). The white precipitate was collected by filtration and washed with acetone and 5% $NaHCO_3$ to give pyridostatin **I** (1.80 g) in 87% yield. ^{1}H NMR (600 MHz, DMSO) δ H 12.21 (s, 2H), 8.53 (s, 4H), 8.49 (d, *J* = 7.8 Hz, 2H), 8.35 (t, *J* = 7.8 Hz, 1H), 8.03 (dd, *J* = 7.8, 3.6 Hz, 4H), 7.82 (t, *J* = 7.8 Hz, 2H), 7.61 (t, *J* = 7.8 Hz, 2H). ^{13}C NMR (150 MHz, DMSO) δ 163.4, 151.2, 148.9, 146.0, 139.9, 138.8, 130.4, 128.0, 126.8, 126.3, 126.0, 125.6, 115.4. HRMS (EI) calculated for $C_{25}H_{17}N_5O_2$ $[M]^+$ *m/z*: 419.1382, found 419.1387.

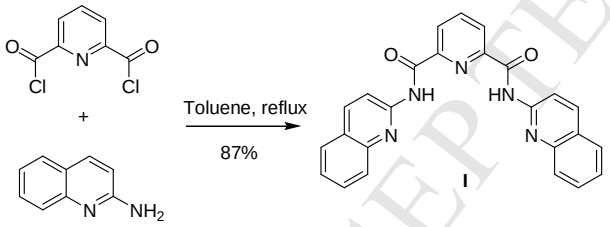

Scheme 2. Synthetic route of pyridostatin **I**.

Preparation of pyridostatin **II**.

Pyridostatin **II** was prepared according to the reported similar procedure,[24] shown as in Scheme 3. The key intermediates **II-a** and **II-b** were prepared starting from chelidamic acid monohydrate and 2-aminoquinolinone, respectively (see Supporting Information).

Step i: Compound **II-a** (326 mg, 1 mmol) and 1-chloro-*N*,*N*′,2-trimethyl-1-propenyl-amine (280 μl, 2.1 mmol) were dissolved in 10 ml DCM at 0 ºC and stirred for 2 h. Triethylamine (347 μl, 2.5 mmol) was added dropwise and the solution stirred for 1 h at 0 ºC. A solution of **II-b** (462 mg, 2 mmol) in 5 ml DCM was added slowly and the resulting mixture stirred at rt overnight. The solvent was removed *in vacuo* and the crude product was crystallized from MeCN yielded a white powder (310 mg, 41.2%) : ^{1}H NMR (400 MHz**,** $CDCl_3$) δ 11.46 (s, 2H), 8.19 (s, 2H), 8.14 (d, *J* = 8.4 Hz, 2H), 7.87 (s, 2H), 7.85 (d, *J* = 8.4 Hz, 2H), 7.67 (t, *J*= 7.6 Hz, 2H), 7.42 (t, *J* = 7.6 Hz, 2H), 5.32 (s, br, 1H), 4.46 (t, *J* = 5.2 Hz, 4H), 4.19 (t, *J* = 4.8 Hz, 2H), 3.62 (t, *J* = 4.8 Hz, 2H), 3.01 (t, *J* = 5.2 Hz, 2H), 2.49 (s, 12H); ^{13}C NMR (100 MHz, $CDCl_3$) δ 167.9, 162.8, 161.9, 158.3, 156.7, 148.8, 148.4, 130.2, 125.5, 122.0, 121.9, 117.9, 112.5, 90.4, 80.1, 68.8, 67.3, 57.8, 46.4, 41.3, 28.6; HRMS (ES) calculated for $C_{40}H_{49}N_8O_7$ $([M + H]^+)$ *m/z*: 753.37197, found 753.37187.

Step ii: The resulting product of step i (300 mg, 0.4 mmol) was dissolved in 4 ml DCM and 2 ml TFA and stirred at rt. for 2h. The solvents was removed in vacuo and the crude product was crystallized from MeOH, and yielded a white solid **II·3CF$_3$COOH** (400 mg, 100%): ^{1}H NMR (400 MHz**,** DMSO) δ 8.36 (d, *J* = 7.6 Hz, 2H), 8.16 (s, 2H), 7.97 (d, *J* = 7.6 Hz, 4H), 7.82 (t, *J* = 6.8 Hz, 2H), 7.57 (t, *J*= 6.8 Hz, 2H), 4.71 (s, 4H), 4.55 (s, 2H), 3.77 (s, 4H), 3.56 (s, 2H), 2.99 (s, 12H); ^{13}C NMR (75 MHz, DMSO) δ 167.1, 163.6, 162.0, 152.6, 151.5, 147.4, 131.4, 127.3, 125.3, 122.9, 119.4, 115.3, 112.8, 95.6, 63.4, 55.6, 43.2, 31.1; HRMS (ES) calculated for $C_{35}H_{41}N_8O_5$ $([M + H]^+)$ *m/z*: 653.31946, found 653.31944.

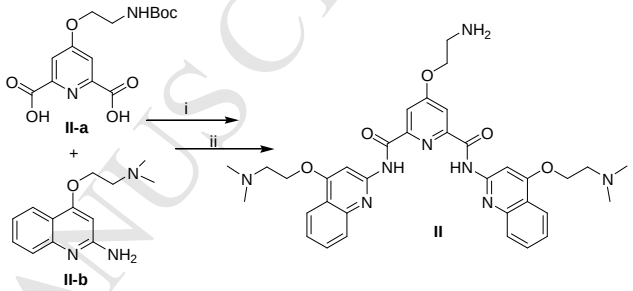

Scheme 3. Synthetic route of pyridostatin **II**. Note: i, 1-chloro-*N*, *N*′, 2-trimethyl-1-propenylamine, DCM, 2 h at 0 ºC then TEA, 1 h at 0 ºC then **II-b**, 12 h, rt. 41%. ii, DCM/ TFA(2: 1), 100%.

The oligonucleotides H22 and H7 were purchased from Invitrogen (Beijing, China), purified by PAGE. All organic reagents were purchased from Beijing J&K Chemical Scientific Company or Beijing InnoChem Science&Technology Co.,Ltd.

4.2. Spectra

NMR Spectra

Chemical shifts were given on the δ scale (ppm) and were referenced to the residual solvent signals; Coupling constants *J* were reported in hertz (Hz). The abbreviations s, d, and m were used for singlet, doublet, and multiplet, respectively.

CD Spectra

CD spectra were collected from 200 to 350 nm on a Jasco-815 automatic recording spectropolarimeter with a 1-cm pathlength quartz cell. Spectra were collected with scan speed of 1000 nm min^{-1}. Each spectrum was the average of three scans.

Fluorescence Spectra

Fluorescence spectra were recorded on a Hitachi F4500 spectrofluorometer (Japan) in a 1-cm pathlength quartz cell at room temperature. Xenon arc lamp was used as the excitation light source. The excitation and emission slits were both 10 nm. Excitation was set at 320 nm, and emission was collected from 335 to 600 nm.

4.3. Binding Mode Models

The 3D coordinates of Hum7 and H22 DNA G-quadruplex structures were retrieved from the RCSB Protein Data Bank (PDB CODE: 1NZM[26] and 3T5E[27]). The G-quadruplex structures were prepared for docking as described.[28] The

pyridostatin **I-II** molecule structures were optimized with MMFF force field using the Discovery Studio 3.5 (Accelrys Software Inc., San Diego). The molecular docking studies were carried out by using the LigandFit module of Discovery Studio 3.5 following the protocols developed for DNA G-quadruplex and ligand docking.[28]

4.4. MTT assays

Three human solid tumor cell lines including human non-small cell lung cancer cell line (A549), human colonic carcinoma cell line (HCT-8), and human hepatocellular carcinoma cell line (BEL-7402) were used in the cytotoxicity test. The cells were cultured in RPMI-1640 medium supplemented with 10% fetal bovine serum (FBS), 100 μg/mL of streptomycin, and 100 μg/mL of penicillin in an atmosphere of 5% CO_2 at 37 °C.

Cytotoxicity of all the compounds were determined by MTT assay (3-(4,5-dimethylthiazol-2-yl)-2,5-diphenyltetrazolium bromide; MTT, Sigma). Briefly, the suspension of 5000 cells per well was plated in 96-well culture plates with culture medium which was incubated for 24 h at 37 °C in a water-atmosphere (5% CO_2). The compounds with desired concentrations were obtained by dissolving in DMSO and diluting with culture medium. And then the diluted solution of complexes was added to the wells, and the cells were incubated for 48 h at 37 °C. After that, 10 μL of a freshly diluted MTT solution (5 mg/mL in PBS) were added to each well and the plates were incubated for 4.5 h. The media with MTT solution were removed with DMSO solution (100 μL). The absorbance was measured at 540 nm with an automatic microplate ELISA reader. The IC_{50} value was determined from the chart of cell viability (%) against dose of complex added (μM).

Acknowledgement

The authors wish to thank the National Natural Science Foudation of China (Grant No. 21302188, 81072576, 91027033) and Chinese Academy of Sciences (Grant No. KJCX2-EW-N06-01 and XDA09030307) for financial support.

Supplementary data

Supplementary datas including synthetic procedures of **II-a** and **II-b**, and optimized models for the complexes: 1) between pyridostatin **I** and G-quadruplex H7; and 2) between pyridostatin **II** and G-quadruplex H22, and characterization datas of all the new compounds.

References

1. de Lange, T. *Genes Dev*. **2005**, *19*, 2100-2110.
2. Organisian, L., and Bryan, T. M. *BioEssays*. **2007**, *29*, 155–165.
3. Kelland, L. R. *Eur. J. Cancer.* **2005**, *41*, 971–979.
4. Neidle, S., Read, M. A. *Biopolymers*, **2001**, *56*, 195–208.
5. Han, H. Y., Hurley, L. H. *Trends Pharmacol Sci*. **2000**, *21*, 136-142.
6. Monchaud, D., Teulade-Fichou, M. P. *Org. Biomol. Chem*. **2008**, *6*, 627-636.
7. Murat, P., Singh, Y., Defrancq, E. *Chem. Soc. Rev.* **2011**, *40*, 5293-5307.
8. Li, Q., Xiang, J. F., Zhang, H., Tang, Y. L. *Curr. Pharm. Design*. **2012**, *18*, 1973-1983.
9. Agrawal, S., Ojha, R. P., Maiti, S. *J. Phys. Chem. B.* 2008, 112, 6828–6836.
10. Chen, Y. W., Yang, D. Z. *Current Protocols in Nucleic Acid Chemistry.* **2012**, 17.5.1-17.5.17.
11. Chu, B., Yuan, G., Zhou, J. Qu Y., Zhu, P. *Drug Dev. Res.* **2008**, *69*, 235–241.
12. Shammas, M. A., Shmookler Reis, R. J., Akiyama, M., Koley, H., Chauhan, D., Hideshima, T., Goyal, R. K., Hurley, L. H., Anderson, K. C., Munshi, N. C. *Mol. Cancer. Ther.* **2003**, *2*, 825–833.
13. Gomez, D., Mergny, J. L., Riou, J. F. *Cancer Res.* **2002**, *62*, 3365–3368.
14. Cookson, J. C., Dai, F., Smith, V., Heald, R. A., Laughton, C. A., Stevens, G., Burger, A. M. *Mol. Pharmacol.* **2005**, *68*, 1551–1558.
15. Bidzinska, J., Cimino-Reale, G., Zaffaroni, N., Folini, M. *Molecules.* **2013**, *18*, 12368-12395.
16. Neidle, S., Balasubramanian, S. *Quadruplex Nucleic Acids, ed. RSC publishing, Cambridge*, **2006**.
17. Parkinson, G. N., Lee, M. P. H., Neidle, S. **2002**, *417*, 876– 880.
18. Luu, K. N., Phan, A. T., Kuryavyi, V., Lacroix, L., Patel, D. J. *J. Am. Chem. Soc.* **2006**, *128*, 9963.
19. Miyoshi, D., Nakao, A., Sugimoto, N. *Biochemistry*. **2002**, *41*, 15017-15024.
20. Zhou, J., Wei, C., Jia, G., Wang, X., Tang, Q., Feng, Z., Li, C. *Biophys. Chem*. **2008**, *136*, 124-127.
21. Heddi, B., Phan, A. T. *J. Am. Chem. Soc*. **2011**, *133*, 9824-9833.
22. Wang, L. X., Xiang, J. F., Tang, Y. L. *Adv. Synth. Catal*. **2015**, *357*, 13-20.
23. Müller, S. Sanders, D. A., Antonio, M. D., Matsis, S., Riou, J. F., Rodriguez, R., Balasubramanian, S. *Org. Biomol. Chem*. **2012**, *10*, 6537-6546.
24. Rodriguez, R., Müller, S., Yeoman, J. A., Trentesaux, C., Riou, J. F., Balasubramanian, S. *J. Am. Chem. Soc.* **2008**, *130*, 15758-15759.
25. Lu, Y. J., Yan, S. C., Chan, F. Y., Zou, L., Chung, W. H., Wong, K. Y. *Chem. Commun*. **2011**, *47*, 4971-4973.
26. Gavathiotis, E., Heald, R. A., Stevens, M. F., Searle, M. S. *J Mol Biol*, **2003**. *334*, 25-36.
27. Collie, G. W., Promontorio, R., Hampel, S. M., Micco, M., Neidle, S., Parkinson, G. N. *J. Am. Chem. Soc*, **2012**, *134*, 2723-2731.
28. Haider, S., Neidle, S. *Methods Mol Biol*, **2010**, *608*, 17-37.
29. The states of the related samples are so complex that we just could provide a possible explanation.

Supporting Information

Pyridostatins Selectively Recognize Two Different Forms of the Human Telomeric G-Quadruplex Structures and Their Antitumor Activities in Vitro

Lixia Wang, Qian Shang, Qian Li, Junfeng Xiang, Yan Liu, Aijiao Guan, Hongxia Sun, Lijia Yu, Yalin Tang*

National Laboratory for Molecular Sciences, Center for Molecular Sciences, State Key Laboratory for Structural Chemistry of Unstable and Stable Species, Institute of Chemistry Chinese Academy of Sciences, Beijing 100190, P.R. China. Fax: 86 10 6252 2090; Tel: 86 10 8261 7304; E-mail: tangyl@iccas.ac.cn

Preparation of the key intermediates of pyridostatin **II**:

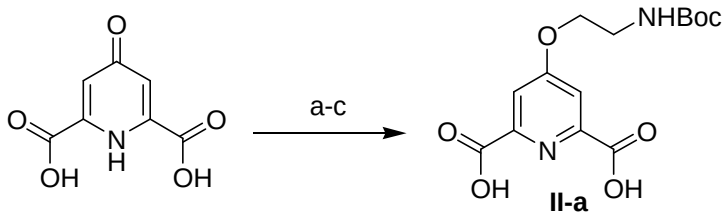

Steps: (a) H_2SO_4, MeOH, reflux. (b) *N*-Boc-ethanolamine, PPh_3, DIAD, THF, rt. (c) aq. NaOH, MeOH, 0 ºC.

Dimethyl-4-[(Tetrahydro-2-pyrany)oxy]-2-6-pyridinedicarboxylate

Chelidamic acid monohydrate (97%, 52.0 g, 0.275 mol) and a catalytic amount of sulfuric acid (10 mL) were dissolved in 700 mL of methanol and the mixture was refluxed for 20 h. After it was cooled to room temperature, the reaction mixture was neutralized with aqueous sodium carbonate solution and then acidified by concentrated hydrochloric acid. Water was added and the resulting mixture was extracted with dichloromethane to give a yellow solid. Crude dimethyl chelidamate was recrystallized from methanol and gave a white solid[1] (39.2 g, 67.6%).[1]H NMR (400MHz, $CDCl_3$) δ 7.33(s, 2H), 4.03 (s, 6H).

Dimethyl-4-(2-*tert*-butoxycarbonylamino-ethoxy)-2,6-pyridinedicarboxylate

Chelidamic acid dimethyl ester (1.06 g, 5 mmol)**,** N-Boc-ethanolamine (1.21 g, 7.5 mmol) and triphenylphosphine (2.62 g, 10 mmol) were dissolved in 30 ml freshly distilled THF and cooled to 0 °C. DIAD (1.52 g, 7.5 mmol) was added dropwise under argon. The mixture was allowed to warm to rt 12 h. The solvent was removed *in vacuo* and the product purified by column chromatography to obtain the title compound (1.07 g, 60.5%) as a white powder[2]. [1]H NMR (400 MHz, $CDCl_3$) δ 7.79 (s, 2H), 4.93 (s, br, 1H), 4.19 (t, *J*= 5.0 Hz, 2H), 3.99 (s, 6H), 3.58 (m, 2H), 1.43 (s, 9H).

4-(2-*tert*-butoxycarbonylamino-ethoxy)-2,6-pyridinedicarboxylic acid II-a:

Compound **2** (354 mg, 1mmol) was dissolved in MeOH (5ml), and then 2 M aq. soln. of NaOH (80mg, 2mmol) was added dropwise at 0 ºC. After finishing the dropping , the reaction mixture was neutralized with concentrated hydrochloric acid to PH ≈ 1.

Water was added and the resulting mixture was extracted with dichloromethane to give a white solid[2] (300 mg, 92.0%). ^{1}H NMR (400 MHz, D_2O) δ H 7.82 (s, 2H), 4.61(t, *J* = 5.6 Hz, 2H), 4.46 (t, *J* = 5.6 Hz, 2H), 1.23 (s, 9H).

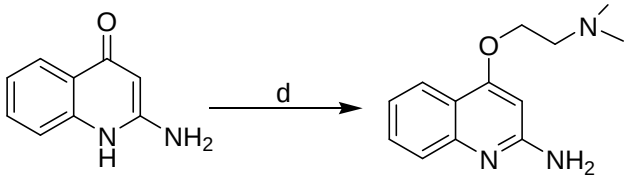

II-b

Step d: N, N-Dimethylethanolamine, PPh_3, DIAD, THF, rt.

4-(Dimethylamino-ethoxy)-quinolin-2-ylamine II-b

2-amino-quinolinone (800 mg, 5 mmol), N,N′-Dimethylethanolamine (667.5 mg, 7.5 mmol) and triphenylphosphine (2.62 g, 10 mmol) were dissolved in 30 ml freshly distilled THF and cooled to 0 °C. DIAD (1.52 g, 7.5 mmol) was added dropwise under argon. The mixture was allowed to warm to rt and stirred for 20h. The solvent was removed *in vacuo* and the product purified by column chromatography to obtain a white powder (539 mg, 46.7%). ^{1}H NMR (400 MHz, $CDCl_3$) δ H 7.98 (d, *J* = 8.0 Hz, 1H), 7.58 (d, *J* = 8.0 Hz, 1H), 7.53 (t, *J* = 7.2 Hz, 1H), 7.21 (t, *J* = 7.2 Hz, 1H), 6.02 (s, 1H), 4.82 (s, br, 2H), 4.19 (t, *J* = 5.6 Hz, 2H), 2.87 (t, *J* = 5.6 Hz, 2H), 2.38 (s, 6H); ^{13}C NMR (100 MHz, $CDCl_3$) δ 162.7, 158.2, 148.4, 130.2, 125.5, 122.0, 121.9, 117.8, 90.0, 67.0, 57.9, 46.2; HRMS (ES) calculated for $C_{13}H_{18}N_3O$ ($[M + H]^+$) *m/z*: 232.14459, found 232.14444.

Reference:

(1). Bradshaw J. S., Colter, M. L., Nakatsuji, Y., Spencer, N. O., Brown, M. F., Izatt, R. M., Arena, G., Tse, P. K., Wilson, B. E., Lamb, J. D., Dalley, N. K. Proton-ionizable crown compounds. 2. Synthesis, complexation properties, and structural studies of macrocyclic polyether-diester ligands containing a 4-hydroxypyridine subcyclic unit. *J. Org. Chem*, **1985**, *50*, 4865-4872.

(2). Rodriguez, R., Müller, S., Yeoman, J. A., Trentesaux, C., Riou, J.-F. and Balasubramanian, S. A novel small molecule that alters shelterin integrity and triggers

a DNA-damage response at telomeres. *J. Am. Chem. Soc*. **2008**, *130*, 15758-15759.

(a)

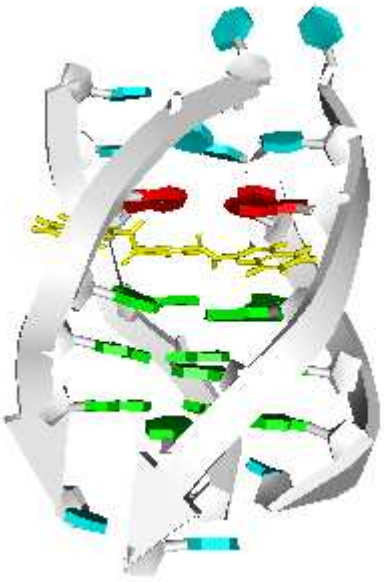

(b)

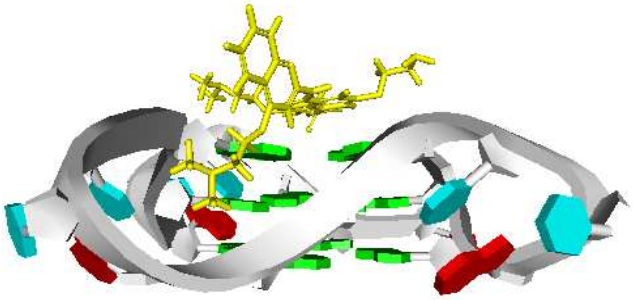

Fig. S1. Optimized models of: (a) complex between pyridostatin **I** and G-quadruplex H7; (b) complex between pyridostatin **II** and G-quadruplex H22. The G is colored in green, the T is colored in light blue, the A is colored in red, and the ligands are colored in yellow.

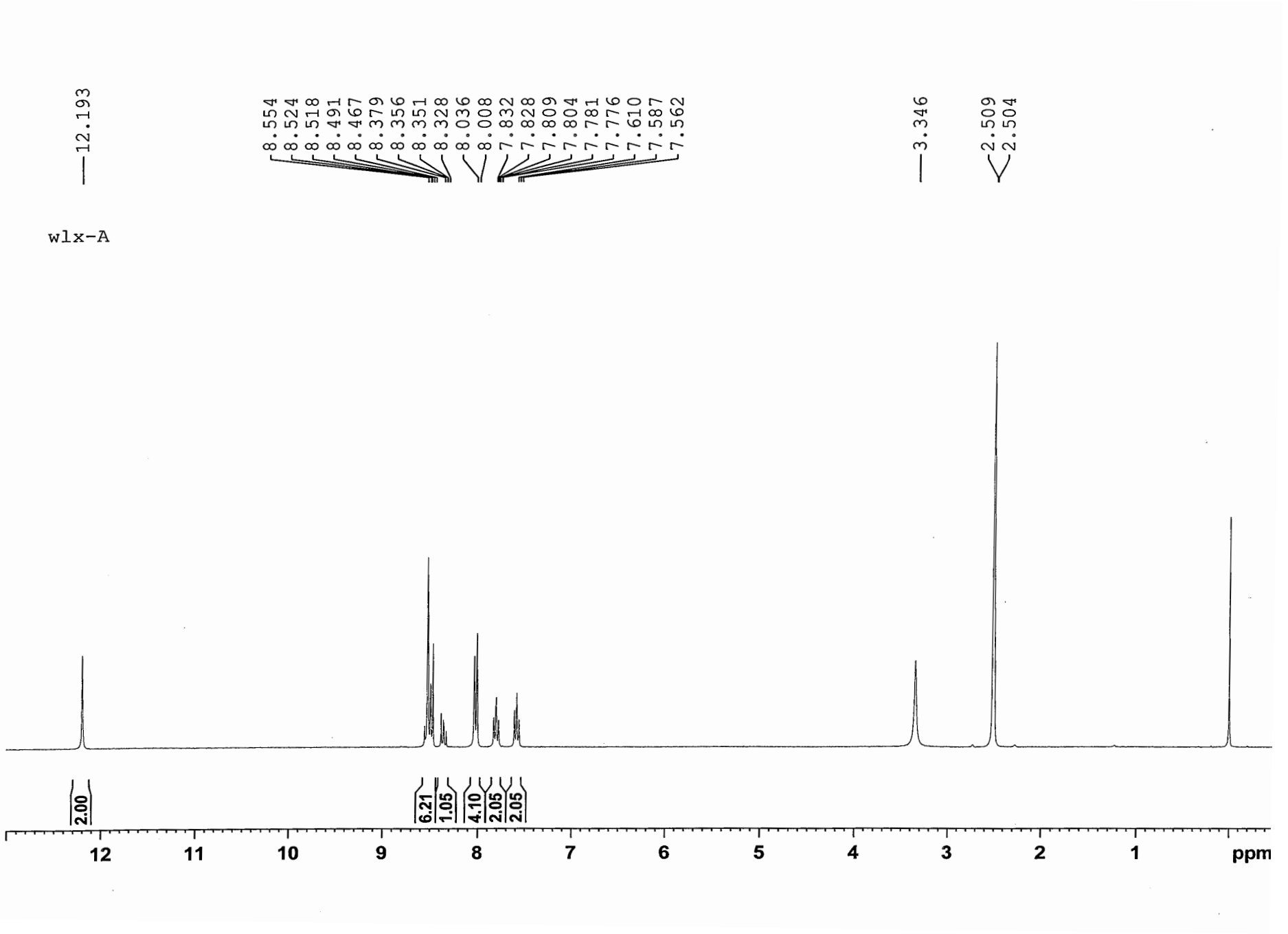
12.193
8.554
8.524
8.518
8.491
8.467
8.379
8.356
8.351
8.328
8.036
8.008
7.832
7.828
7.809
7.804
7.781
7.776
7.610
7.587
7.562
3.346
2.509
2.504
wlx-A
2.00
6.21
1.05
4.10
2.05
2.05
12
11
10
9
8
7
6
5
4
3
2
1
ppm

13C NMR
wlx-A
20130118

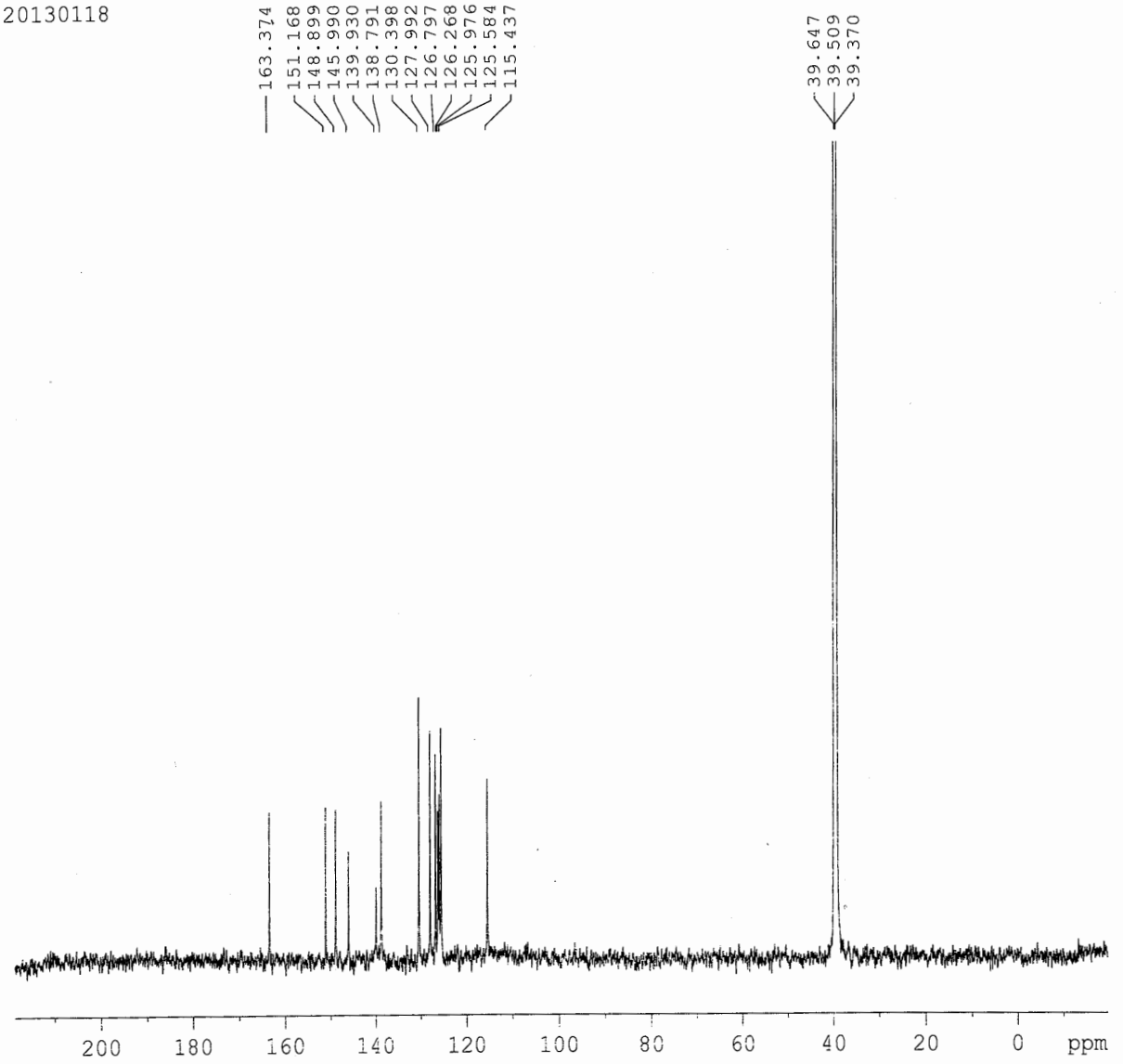

NAME	zhangmiao
EXPNO	103
PROCNO	1
Date_	20130118
Time	17.01
INSTRUM	spect
PROBHD	5 mm PATBO BB-
PULPROG	zgpg30
TD	65536
SOLVENT	DMSO
NS	324
DS	0
SWH	35971.223 Hz
FIDRES	0.548877 Hz
AQ	0.9110143 sec
RG	32768
DW	13.900 usec
DE	6.50 usec
TE	298.0 K
D1	2.00000000 sec
D11	0.03000000 sec
TD0	1
======== CHANNEL f1 ========	
NUC1	13C
P1	14.50 usec
PL1	-2.00 dB
PL1W	119.43215179 W
SFO1	150.9178988 MHz
======== CHANNEL f2 ========	
CPDPRG2	waltz16
NUC2	1H
PCPD2	88.00 usec
PL2	2.00 dB
PL12	19.45 dB
PL13	18.80 dB
PL2W	15.84893227 W
PL12W	0.28510177 W
PL13W	0.33113119 W
SFO2	600.1324650 MHz
SI	32768
SF	150.9028808 MHz
WDW	EM
SSB	0
LB	10.00 Hz
GB	0
PC	1.40

WLX-A **GCT CA127 Micronass UK**

141208-5 97 (1.634) Cm (95:98-1:8) TOF MS EI+ 2.91e3

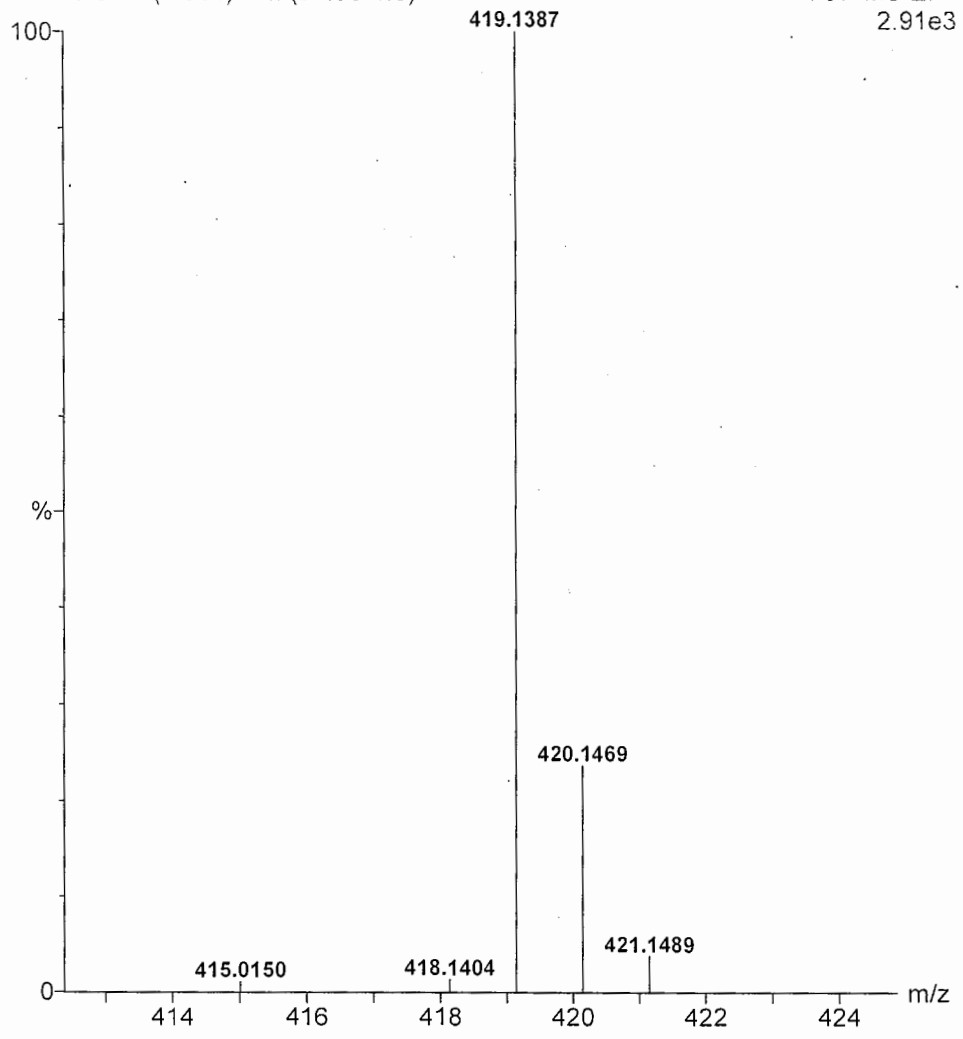

Elemental Composition Report

Tolerance = 10.0 PPM / DBE: min = -1.5, max = 50.0
Isotope cluster parameters: Separation = 1.0 Abundance = 1.0%

Monoisotopic Mass, Odd and Even Electron Ions
14 formula(e) evaluated with 1 results within limits (up to 50 closest results for each mass)

Minimum:	80.00				-1.5		
Maximum:	100.00		200.0	10.0	50.0		
Mass	RA	Calc. Mass	mDa	PPM	DBE	Score	Formula
419.1387	100.00	419.1382	0.5	1.1	20.0	1	C25 H17 N5 O2

wlx0320

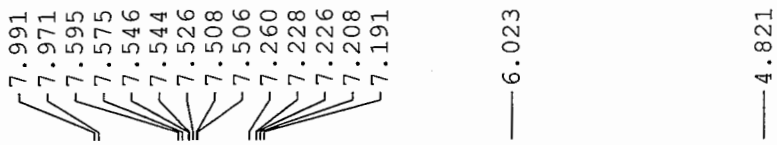

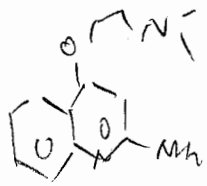

Current Data Parameters

NAME	proton
EXPNO	17
PROCNO	1

F2 - Acquisition Parameters

Date_	20130320
Time	15.55
INSTRUM	spect
PROBHD	5 mm PADUL 13C
PULPROG	zg30
TD	32768
SOLVENT	CDC13
NS	16
DS	0
SWH	12019.230 Hz
FIDRES	0.366798 Hz
AQ	1.3631988 sec
RG	128
DW	41.600 usec
DE	6.50 usec
TE	294.3 K
D1	2.00000000 sec
TD0	1

======== CHANNEL f1 ========

NUC1	1H
P1	12.60 usec
PLW1	13.06000042 W
SFO1	400.1320007 MHz

F2 - Processing parameters

SI	65536
SF	400.1300177 MHz
WDW	EM
SSB	0
LB	0.50 Hz
GB	0
PC	1.00

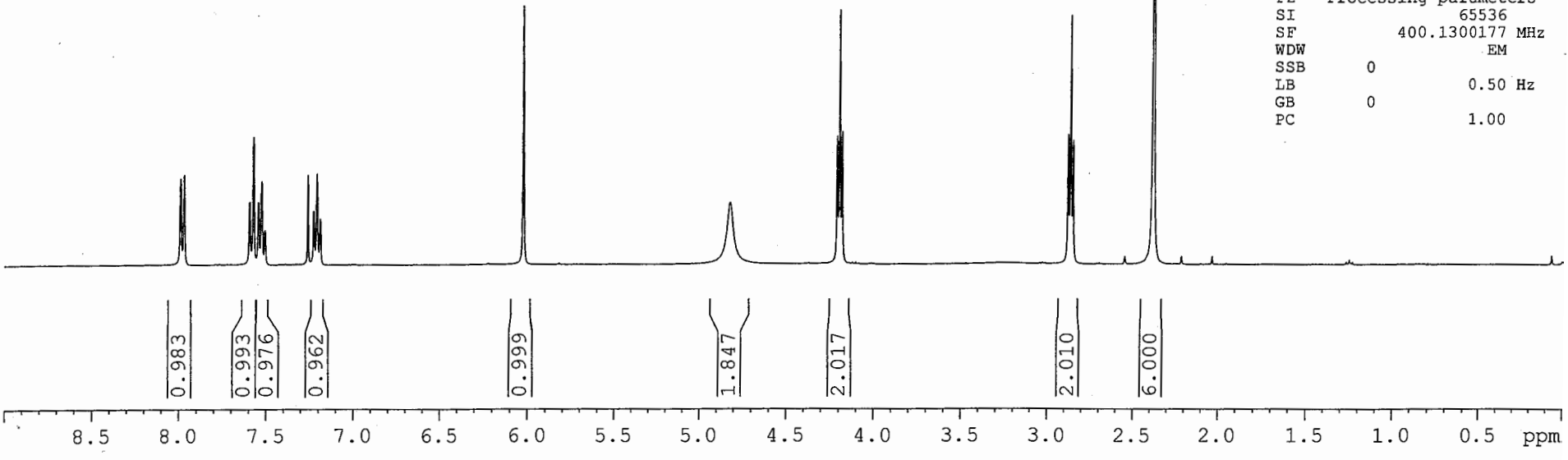

wlx0320

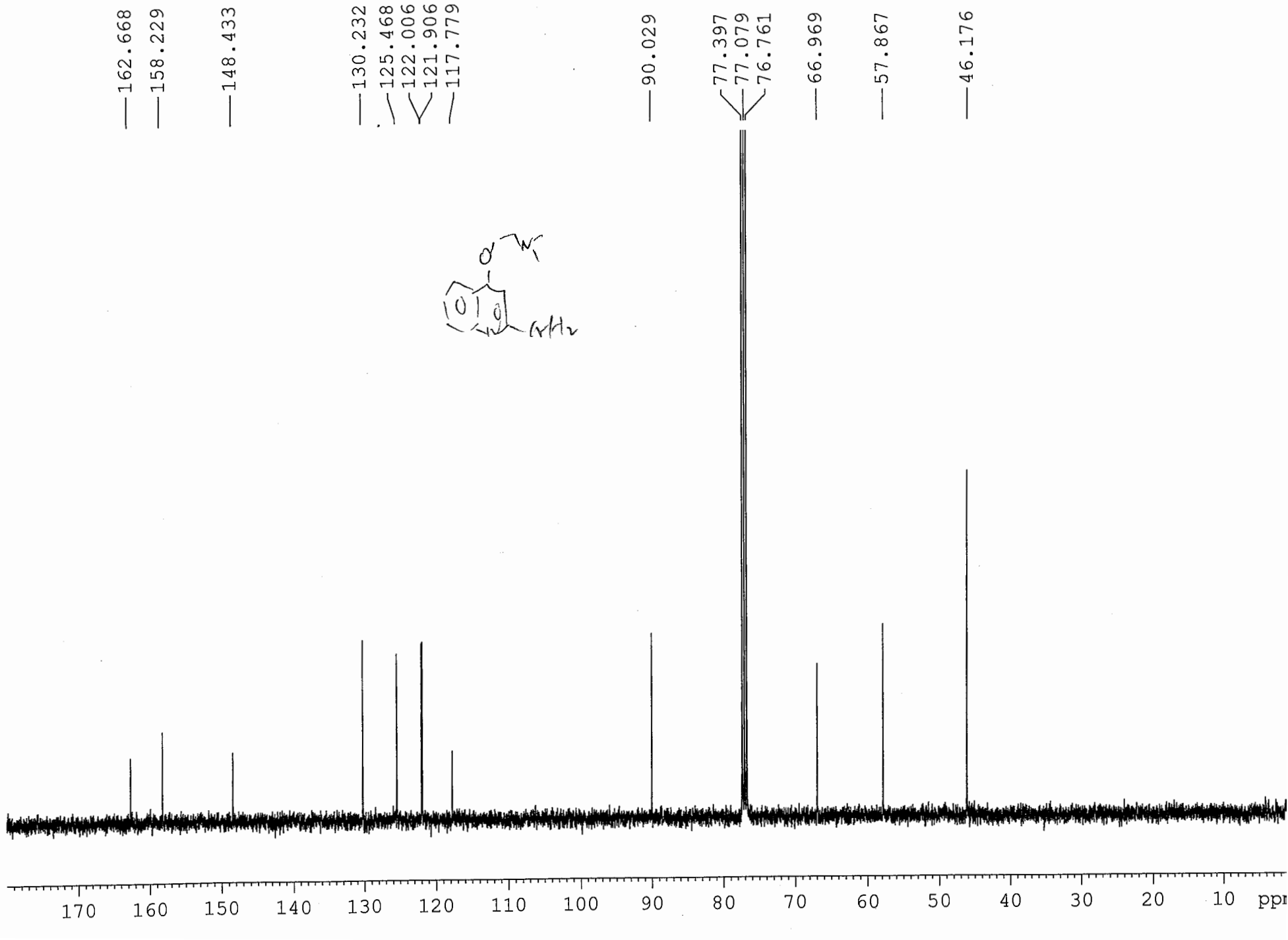
162.668
158.229
148.433
130.232
125.468
122.006
121.906
117.779
90.029
77.397
77.079
76.761
66.969
57.867
46.176
170
160
150
140
130
120
110
100
90
80
70
60
50
40
30
20
10
ppm

WLX-1 #9-10 RT: 0.09-0.10 AV: 2 NL: 5.60E6
T: FTMS {1,1} + p ESI Full ms [50.00-1000.00]

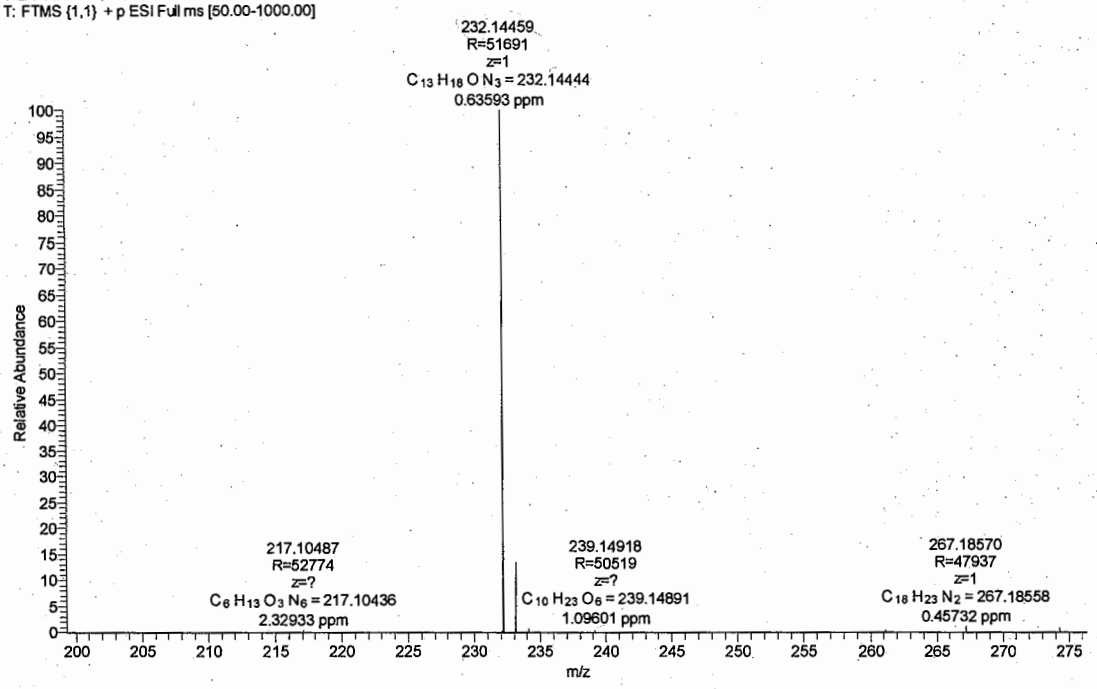

WLX-1 #9-10 RT: 0.09-0.10 AV: 2 NL: 2.14E7
T: FTMS {1,1} + p ESI Full ms [50.00-1000.00]

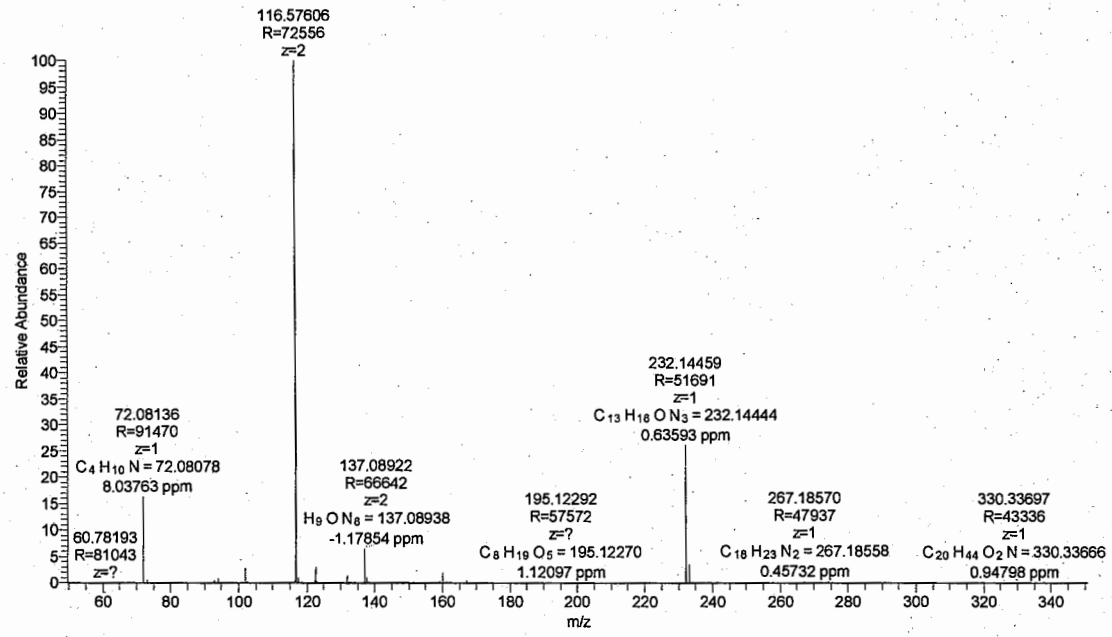

1.935
3.954
3.933
2.067
2.000
0.907
3.924
2.079
2.205
6.332
4.657
12.135
9.604
11.462
8.185
8.151
8.130
7.873
7.858
7.837
7.687
7.669
7.650
7.442
7.423
7.405
7.260
5.318
4.471
4.457
4.444
4.197
4.186
4.173
3.624
3.613
3.079
3.018
3.005
2.992
2.485
1.484
11 10 9 8 7 6 5 4 3 2 1 ppm
wlx1106

167.65
167.54
162.22
158.71
156.16
153.98
144.62
131.18
122.35
122.17
116.55
111.69
91.11
78.43
67.69
65.96
56.62
44.89
40.63
40.35
40.08
39.80
39.52
39.24
38.96
28.62
wlx-e/
BRUKER
180
170
160
150
140
130
120
110
100
90
80
70
60
50
40
30
ppm

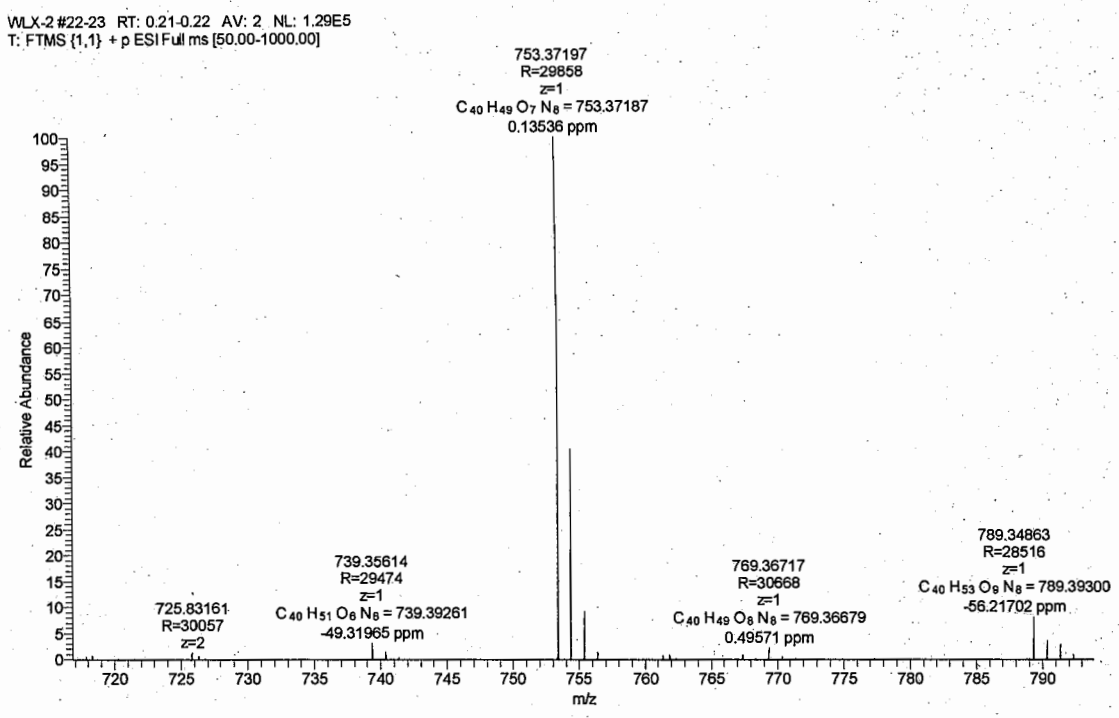
WLX-2 #22-23 RT: 0.21-0.22 AV: 2 NL: 1.29E5
T: FTMS {1,1} + p ESI Full ms [50.00-1000.00]
753.37197
R=29858
z=1
C40 H49 O7 N8 = 753.37187
0.13536 ppm
725.83161
R=30057
z=2
739.35614
R=29474
z=1
C40 H51 O6 N8 = 739.39261
-49.31965 ppm
769.36717
R=30668
z=1
C40 H49 O8 N8 = 769.36679
0.49571 ppm
789.34863
R=28516
z=1
C40 H53 O9 N8 = 789.39300
-56.21702 ppm
Relative Abundance
m/z

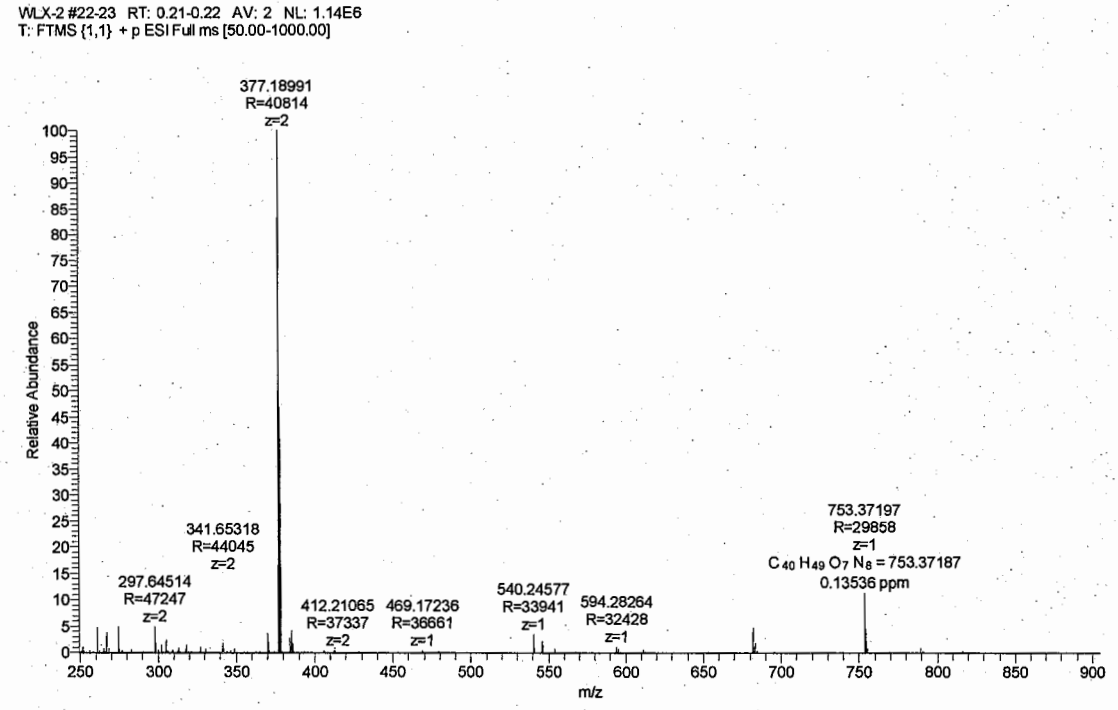
WLX-2 #22-23 RT: 0.21-0.22 AV: 2 NL: 1.14E6
T: FTMS {1,1} + p ESI Full ms [50.00-1000.00]
377.18991
R=40814
z=2
341.65318
R=44045
z=2
297.64514
R=47247
z=2
412.21065
R=37337
z=2
469.17236
R=36661
z=1
540.24577
R=33941
z=1
594.28264
R=32428
z=1
753.37197
R=29858
z=1
C40 H49 O7 N8 = 753.37187
0.13536 ppm
Relative Abundance
m/z

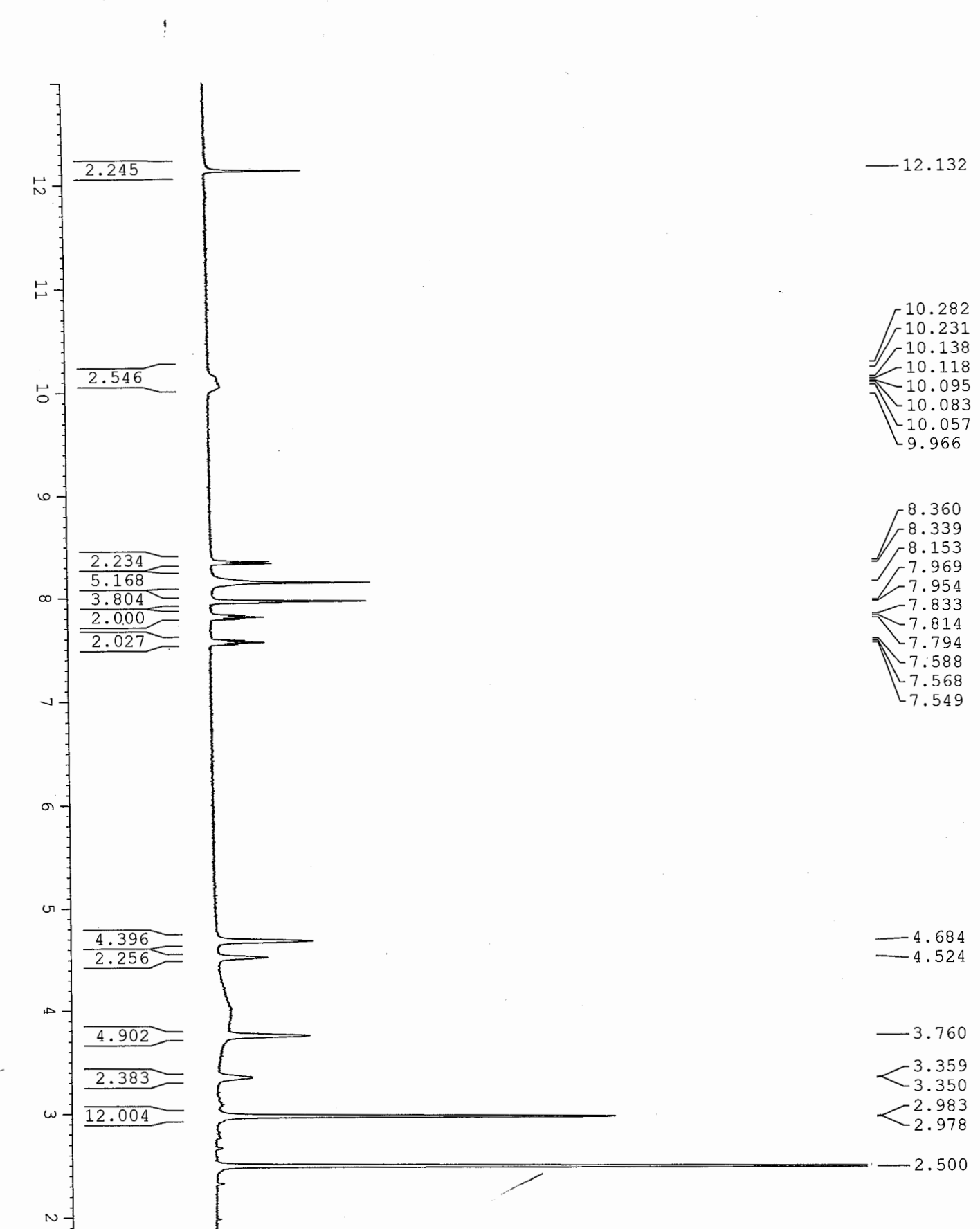
2.245
2.546
2.234
5.168
3.804
2.000
2.027
4.396
2.256
4.902
2.383
12.004
12.132
10.282
10.231
10.138
10.118
10.095
10.083
10.057
9.966
8.360
8.339
8.153
7.969
7.954
7.833
7.814
7.794
7.588
7.568
7.549
4.684
4.524
3.760
3.359
3.350
2.983
2.978
2.500
12
11
10
9
8
7
6
5
4
3
2

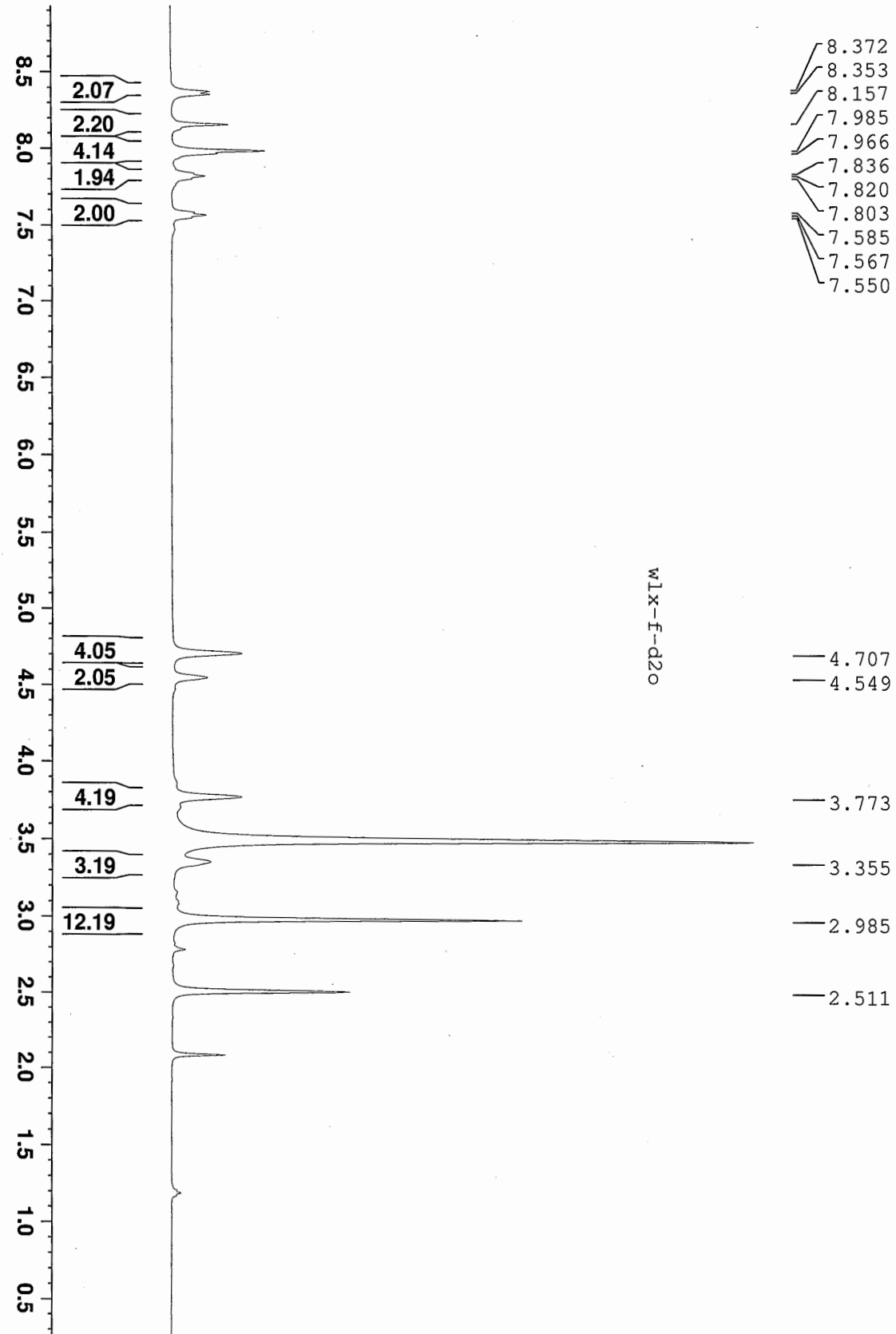
8.372
8.353
8.157
7.985
7.966
7.836
7.820
7.803
7.585
7.567
7.550
2.07
2.20
4.14
1.94
2.00
4.05
2.05
4.19
3.19
12.19
wlx-f-d2o
4.707
4.549
3.773
3.355
2.985
2.511
8.5
8.0
7.5
7.0
6.5
6.0
5.5
5.0
4.5
4.0
3.5
3.0
2.5
2.0
1.5
1.0
0.5

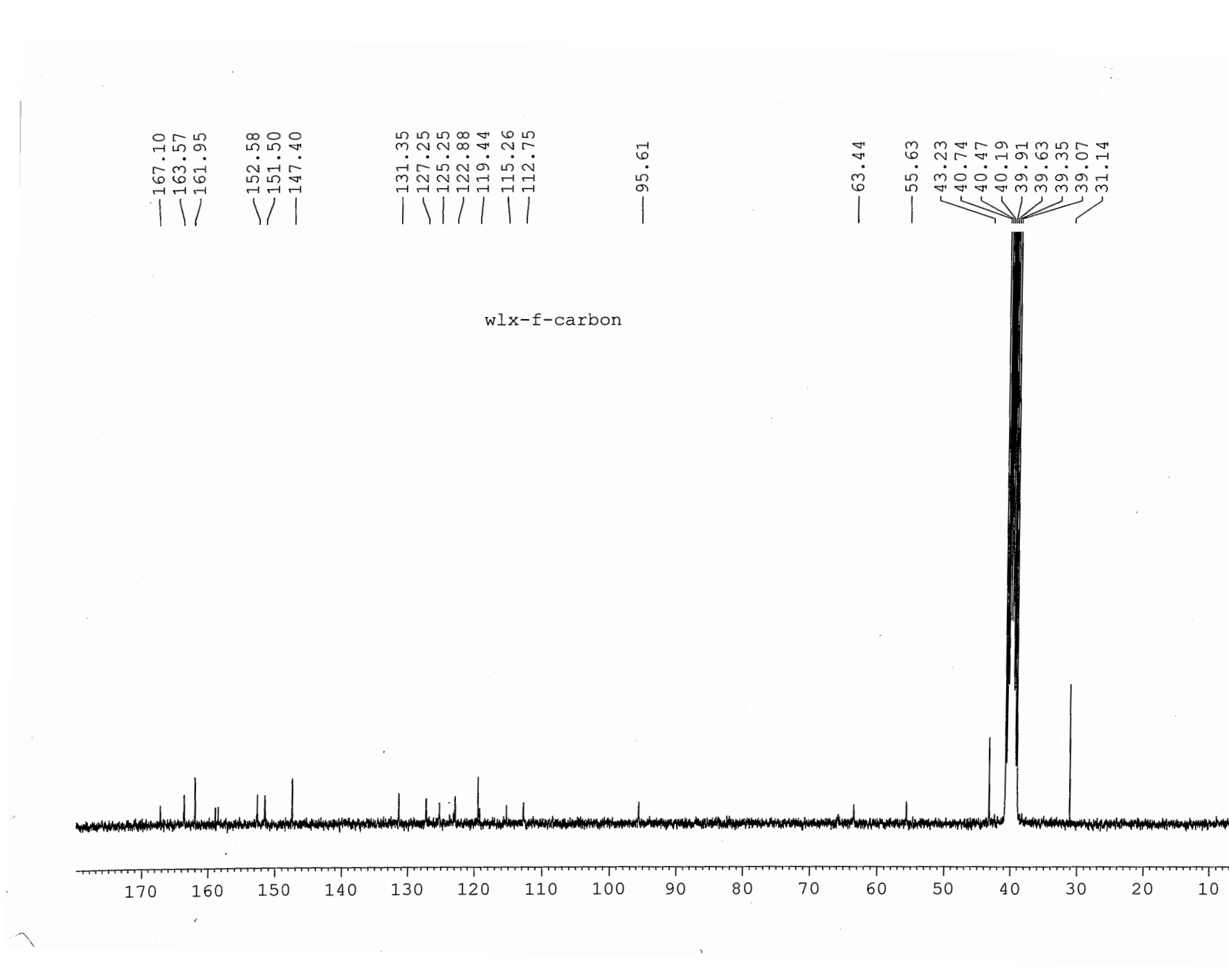
167.10
163.57
161.95
152.58
151.50
147.40
131.35
127.25
125.25
122.88
119.44
115.26
112.75
95.61
63.44
55.63
43.23
40.74
40.47
40.19
39.91
39.63
39.35
39.07
31.14
wlx-f-carbon
170
160
150
140
130
120
110
100
90
80
70
60
50
40
30
20
10

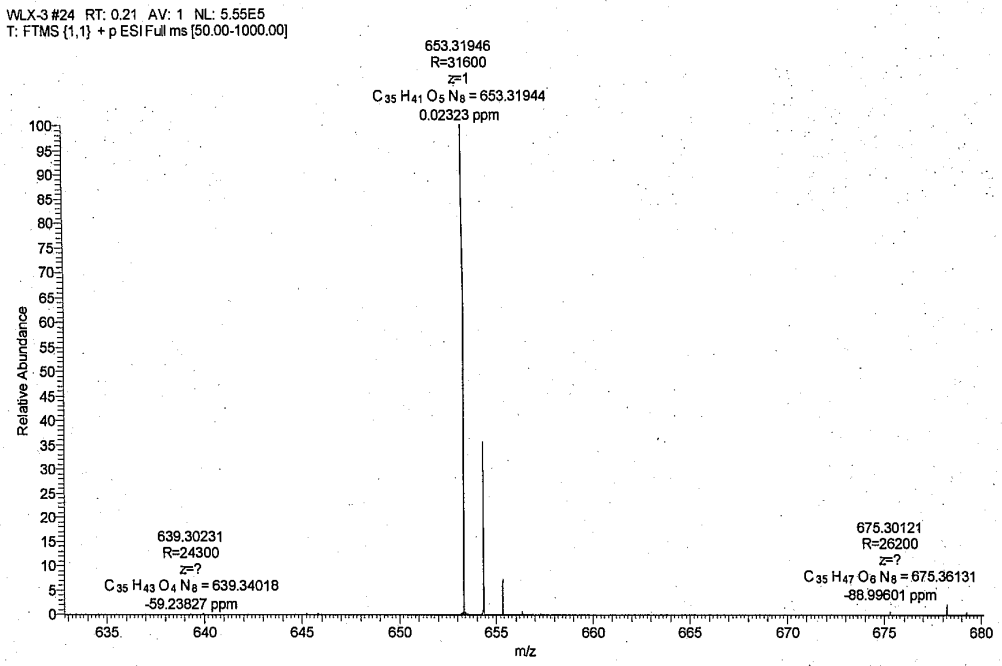
WLX-3 #24 RT: 0.21 AV: 1 NL: 5.55E5
T: FTMS {1,1} + p ESI Full ms [50.00-1000.00]
653.31946
R=31600
z=1
C35 H41 O5 N8 = 653.31944
0.02323 ppm
639.30231
R=24300
z=?
C35 H43 O4 N8 = 639.34018
-59.23827 ppm
675.30121
R=26200
z=?
C35 H47 O6 N8 = 675.36131
-88.99601 ppm
Relative Abundance
m/z

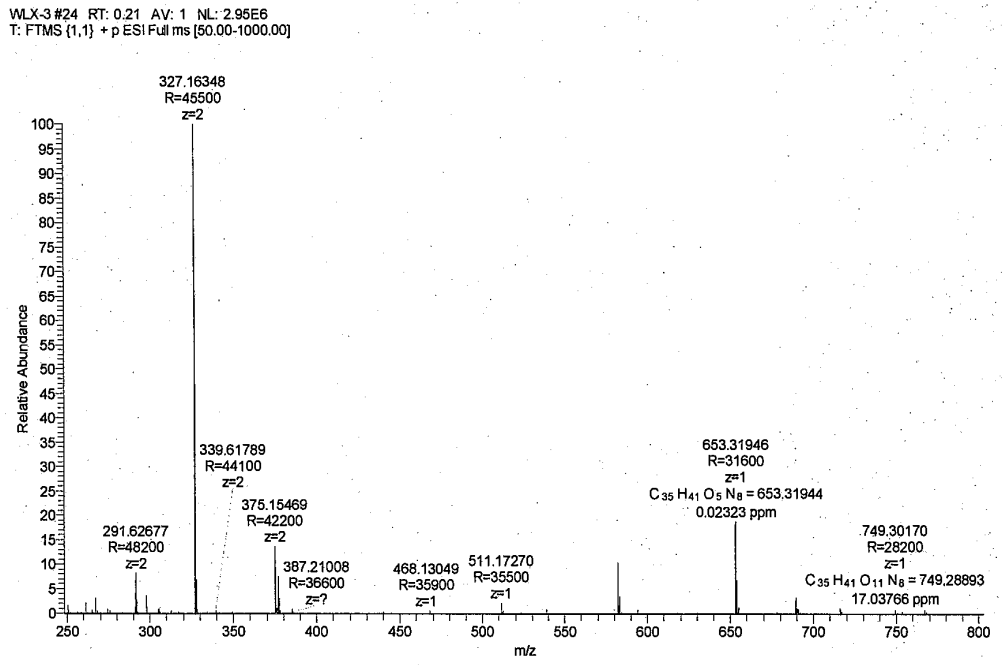
WLX-3 #24 RT: 0.21 AV: 1 NL: 2.95E6
T: FTMS {1,1} + p ESI Full ms [50.00-1000.00]
327.16348
R=45500
z=2
339.61789
R=44100
z=2
375.15469
R=42200
z=2
291.62677
R=48200
z=2
387.21008
R=36600
z=?
468.13049
R=35900
z=1
511.17270
R=35500
z=1
653.31946
R=31600
z=1
C35 H41 O5 N8 = 653.31944
0.02323 ppm
749.30170
R=28200
z=1
C35 H41 O11 N8 = 749.28893
17.03766 ppm
Relative Abundance
m/z